Electronic Supplementary Information

A Hydrophobic-superoleophilic 2D Zr-based Alkyne-rich Metal-Organic Framework for Oil/Water Separation and Solar-assisted Oil Evaporation

Qian-Ru Luo[§], Yuan-Hui Zhong[§], Lai-Hon Chung, Zhixin Jiang, Qia-Chun Lin, Xin-Ke Xu, Xinhe Ye, Wei-Ming Liao and Jun He**

School of Chemical Engineering and Light Industry, Guangdong University of Technology, Guangzhou 510006, China

* Corresponding author.

E-mail: junhe@gdut.edu.cn, laihonchung@gdut.edu.cn

[§]*These authors contributed equally.*

Table of contents

General procedure. S4

Scheme S1. The synthetic scheme for H_2**L1**. S5

Experimental procedures. S5-S11

^{1}H and ^{13}C NMR spectra of the ligand H_2L1 and intermediates. S6-S11

Fig. S1. The ^{1}H NMR spectrum of **SM3**. S6

Fig. S2. The ^{13}C NMR spectrum of **SM3**. S6

Fig. S3. The ^{1}H NMR spectrum of **SM4**. S7

Fig. S4. The ^{13}C NMR spectrum of **SM4**. S7

Fig. S5. The ^{1}H NMR spectrum of **SM5**. S8

Fig. S6. The ^{13}C NMR spectrum of **SM5**. S8

Fig. S7. The ^{1}H NMR spectrum of Me_2**L1**. S9

Fig. S8. The ^{13}C NMR spectrum of Me_2**L1**. S9

Fig. S9. The ^{1}H NMR spectrum of H_2**L1**. S10

Fig. S10. The ^{13}C NMR spectrum of H_2**L1**. S10

Fig. S11. A mass spectrum (ESI) of compound H_2**L1**. S11

Synthesis and activation of ZrL1. S11

Structure simulation. S11

Fig. S12. FT-IR spectra of ligand, as made sample and activated sample of Zr**L1**. S12

Fig. S13. ^{1}H NMR spectra of the filtrate of Zr**L1** digested in HF/DMSO-d_6 and H_2**L1** in DMSO-d_6. S12

Fig. S14. Thermogravimetric analysis plots of activated Zr**L1** in N_2 and air. S12

Fig. S15. N_2 sorption isotherm at 77 K and QSDFT analysis for Zr**L1**. S13

Fig. S16. CO_2 sorption isotherm at 175 K and QSDFT analysis for Zr**L1**. S13

Fig. S17. PXRD patterns of Zr**L1** before and after gas sorption measurement. S13

Fig. S18. XPS spectra of Zr**L1**. S14

Fig. S19. EDS elemental analysis results of Zr**L1**. S14

Fig. S20. PXRD patterns of Zr**L1** for chemical stability measurement. S14

Fig. S21. Photographs of the droplets of saline water, acidic solution, alkaline solution and dichloromethane on Zr**L1** powder with contact angle values. S15

Fig. S22. Photographs of droplet profiles on the surface of original PU Sponge with contact angle values. S15

Fig. S23. FT-IR spectra of Zr**L1**, PU and Zr**L1**@PU. S15

Table S1. Loading of Zr**L1**@PU. S15

Fig. S24. Kubelka-Munk-transformed reflectance spectra for solid samples of PU, Zr**L1** and Zr**L1**@PU. S16

Fig. S25. The compression and detachment of organic droplets and water droplets on the surface of Zr**L1**@PU. S16

Fig. S26. Photographs of the droplets of saline water, acidic solution, alkaline solution on Zr**L1**@PU with contact angle values. S16

Fig. S27. SEM images of original PU Sponge and Zr**L1**@PU samples with different loadings of Zr**L1**. S17

Fig. S28. Organic solvent-absorption capacity of the Zr**L1**@PU. S17

Fig. S29. Photographs of Zr**L1**@PU. S18
Table S2. Absorption capacity, separation efficiency and flux densities of different kinds of oil. S18
Fig. S30. The separation efficiency of Zr**L1**@PU with different loading in dichloromethane/water mixture; dichloromethane/water mixture and dichloromethane/sea water mixture for 9 cycles of separation; Zr**L1**@PU in dichloromethane/water mixture as a function of operation time duration. S19
Fig. S31. The dichloromethane-water mixture separation process. S19
Fig. S32. The ethyl acetate-water mixture separation process. S20
Fig. S33. Photothermal conversion behaviour of Zr**L1**. S20
Fig. S34. Schematic diagram of photo-driven solvent evaporation experimental set-up. S21
Fig. S35. Photo-driven distillation tests of Zr**L1**@PU. S21
Fig. S36. FT-IR spectra and PXRD patterns of Zr**L1** recovered from Zr**L1**@PU after five photothermal conversion cycles, oil/water separation and solvent evaporation experiment. S22
Table S3. Comparisons of absorption capacities and separation efficiency of previously reported absorbents with Zr**L1**@PU. S22-S23
References. S24

General procedure.

All the starting materials, reagents, and solvents were purchased from commercial sources (J&K, Zhengzhou Alfa and Acros) and used without additional purification. Elemental analysis was obtained with a Elementar Vario EL cube elemental analyser. Powder X-ray diffraction (PXRD) patterns were collected on a Rigaku Smart lab diffractometer with Cu Kα radiation (λ = 1.5418 Å) at room temperature. The X-ray tube operated at a voltage of 40 kV and a current of 15 mA. FT-IR spectra (KBr pellet) in the range 400–4000 cm^{-1} were recorded on a Thermo Fisher iS50R FT-IR spectrophotometer. Solution ^{1}H NMR and ^{13}C NMR spectra were recorded on a 400 MHz Bruker superconducting magnet high-field NMR spectrometer at room temperature, with tetramethylsilane (TMS) as the internal standard. Chemical shifts (δ) are expressed in ppm relative to the residual solvent (*e.g.,* chloroform ^{1}H: 7.26 ppm, ^{13}C: 77.0 ppm) reference. Coupling constants are expressed in hertz (Hz). XPS spectra was carried out by a SACEnning Auger/X-ray Photoelectron Spectroscopy System (PHI 5802). Thermogravimetric analysis (TGA) was carried out on a Netzsch STA449F5 thermal analyser from 30 ℃ to 900 ℃ at a heating rate of 10 ℃ min^{-1} under N_2 atmosphere. The sample was then held at vacuum until the analysis was run. The porosity and surface area analysis were performed using a Quantachrome Autosorb iQ gas sorption analyser. The sample was outgassed at 0.03 torr with a 5 ℃/min ramp to 100 ℃ and held at this temperature for 12 hours. The sample was then held at vacuum until the analysis was run. Pawley refinement was carried out using Materials Studio Software. The morphology of the samples was investigated using scanning electron microscopy (SEM, SIGMA 500, ZEISS, Germany). All the water contact angle measurements were carried out by Hol-marc, HO-IOD-CAN-018 equipment. Diffuse reflection spectra were collected in the UV-visible near infra-red spectrophotometer with Integrating Sphere (SHIMADZU UV-3600 Plus).

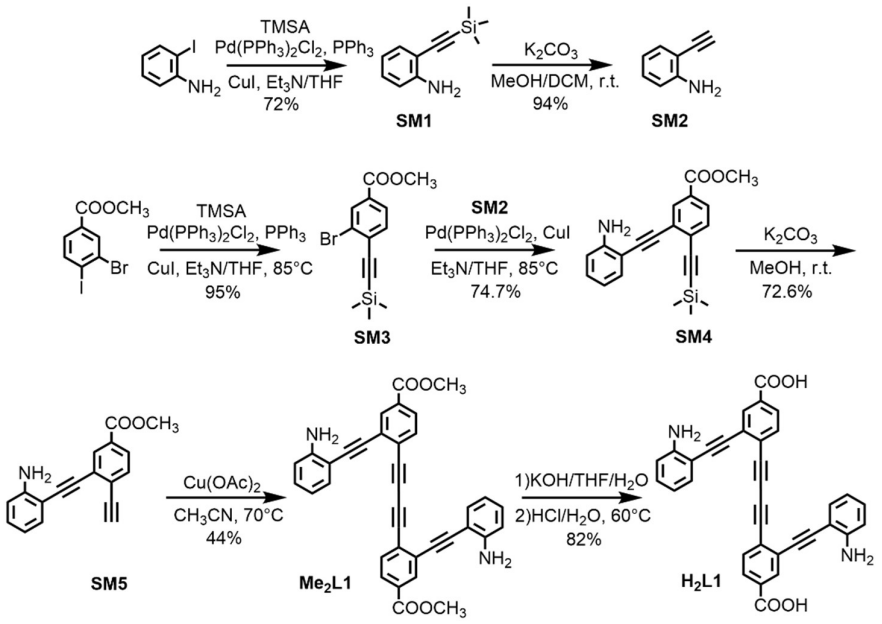

Scheme S1. The synthetic scheme for H_2**L1**.

Experimental procedures.

Synthesis of 2-((trimethylsilyl)ethynyl)aniline (SM1), 2-ethynylaniline (SM2).
SM1 and **SM2** were prepared in accordance with previously reported procedure[1]. The ^{1}H NMR and ^{13}C NMR spectra were in agreement with the literature.

Synthesis of methyl 3-bromo-4-((trimethylsilyl)ethynyl)benzoate (SM3).
Methyl 3-bromo-4-iodobenzoate (5.0 g, 14.7 mmol), triphenylphosphine (384.65 mg, 1.5 mmol), bis(triphenylphosphine) palladium(II) chloride (308.8 mg, 0.43 mmol) and copper(I) iodide (83.8 mg, 0.43 mmol) were added to 25 mL pressure tube. Triethylamine (4 mL) and tetrahydrofuran (THF, 4 mL) each previously purged by bubbling N_2 gas for 5 minutes, were then transferred into the tube *via* a cannula. Under the N_2 atmosphere, trimethylsilylacetylene (TMSA, 1.73 g, 17.6 mmol) was added, sealed and reacted at 85 ℃ for 3 hours. After cooling to room temperature, the solvents were removed by a rotary evaporation and the residue was purified by silica gel column chromatography (eluent: petroleum ether/ethyl acetate, 20:1, v/v) to yield compound **SM3** as yellow solid (4.33 g, 95% yield based on raw materials). ^{1}H NMR (400 MHz, $CDCl_3$): δ = 8.22 (s, 1H), 7.89 (d, 1H), 7.53 (d, 1H), 3.91 (s, 3H), 0.28 (s, 9H). ^{13}C NMR (100 MHz, $CDCl_3$): δ = 165.27, 133.40, 133.37, 130.92, 129.64, 127.90, 125.69, 103.33, 102.44, 52.51, –0.21.

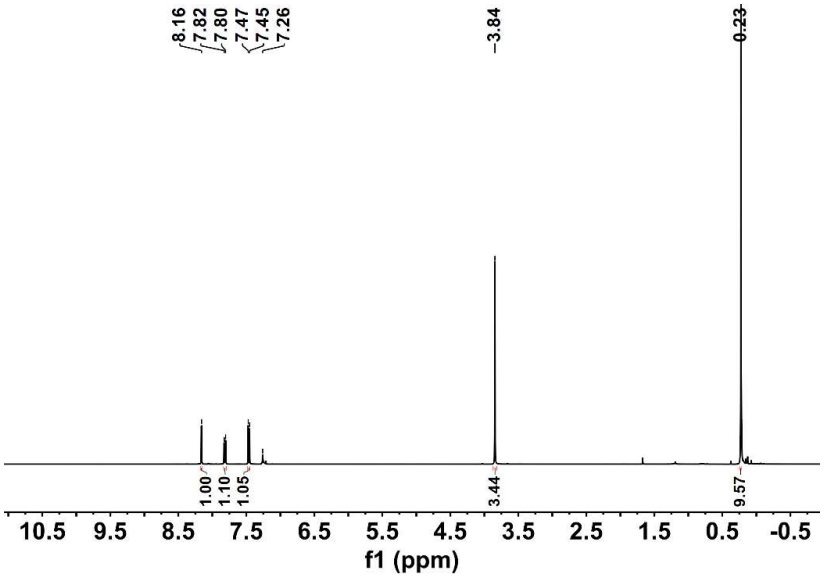

Fig. S1. The ^{1}H NMR spectrum of **SM3** ($CDCl_3$, 400 MHz).

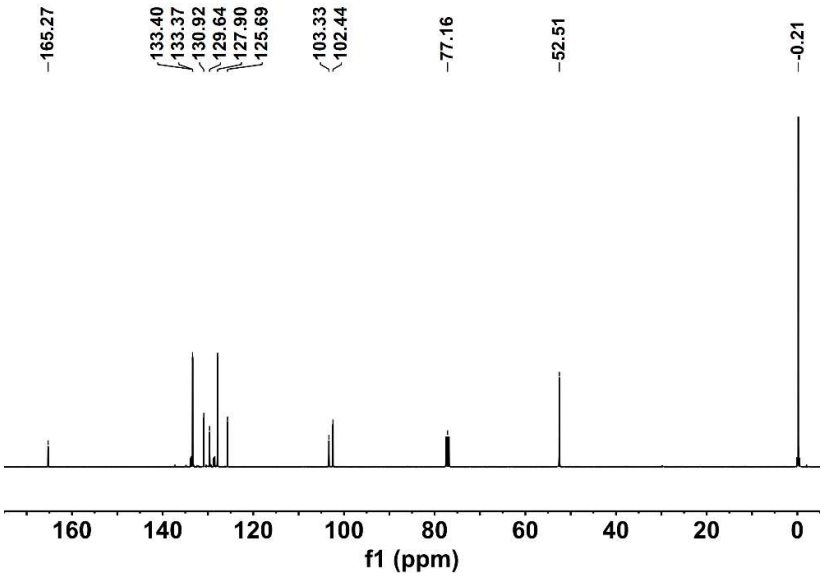

Fig. S2. The ^{13}C NMR spectrum of **SM3** ($CDCl_3$, 100 MHz).

Synthesis of methyl 3-((2-aminophenyl)ethynyl)-4-((trimethylsilyl)ethynyl)benzoate (SM4).

A mixture of compound **SM3** (2.0 g, 6.4 mmol), compound **SM2** (3.76 g, 32.1 mmol), bis(triphenylphosphine) palladium(II) chloride (135.3 mg, 0.2 mmol), and copper(I) iodide (36.7 mg, 0.2 mmol) were added to a 50-mL Schlenk tube and then the tube was connected to a vacuum manifold, evacuated and back-filled with N_2 gas for three times. Triethylamine (14 mL) and THF (7 mL), each previously purged by bubbling N_2 gas for 5 minutes, were then transferred into the tube *via* a cannula. The tube was screw-capped and the reaction solution was stirred at 85 ℃ under N_2 protection for 7 hours. After cooling to room temperature, the solvents were removed by a rotary evaporation and the residue was purified by silica gel column

chromatography (eluent: *n*-hexane/ethyl acetate, 10:1, v/v) to yield compound **SM4** as orange oily liquid (1.67 g, 74.7% yield based on compound **SM3**). ^{1}H NMR (400 MHz, $CDCl_3$): δ = 8.19 (s, 1H), 7.91 (d, 1H), 7.58 (d, 1H), 7.41 (d, 1H), 7.16 (t, 1H), 6.74 (d, 1H), 6.70 (t, 1H), 3.93 (s, 3H), 0.29 (s, 9H). ^{13}C NMR (100 MHz, $CDCl_3$): δ = 166.00, 148.30, 132.83, 132.66, 132.34, 130.35, 129.87, 129.01, 128.35, 126.34, 117.82, 114.31, 107.25, 103.50, 101.88, 92.76, 91.34, 52.44, 0.05.

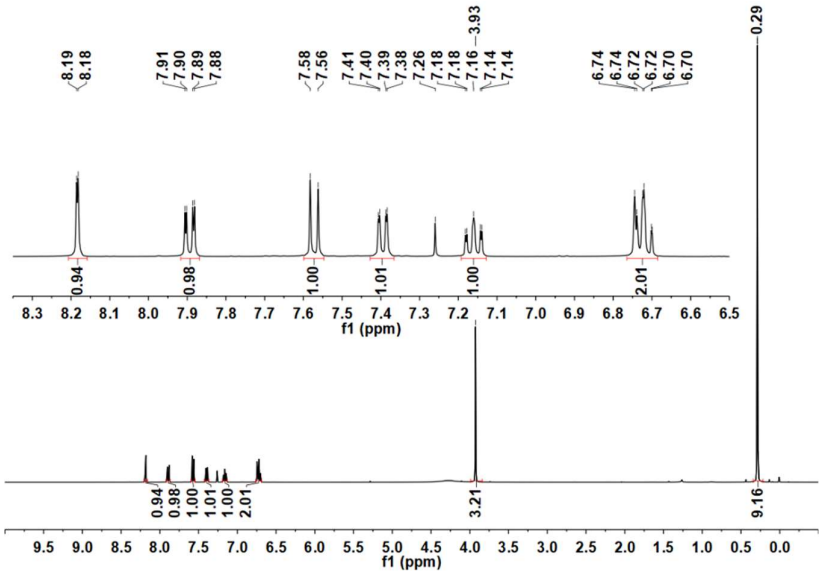

Fig. S3. The ^{1}H NMR spectrum of **SM4** ($CDCl_3$, 400 MHz).

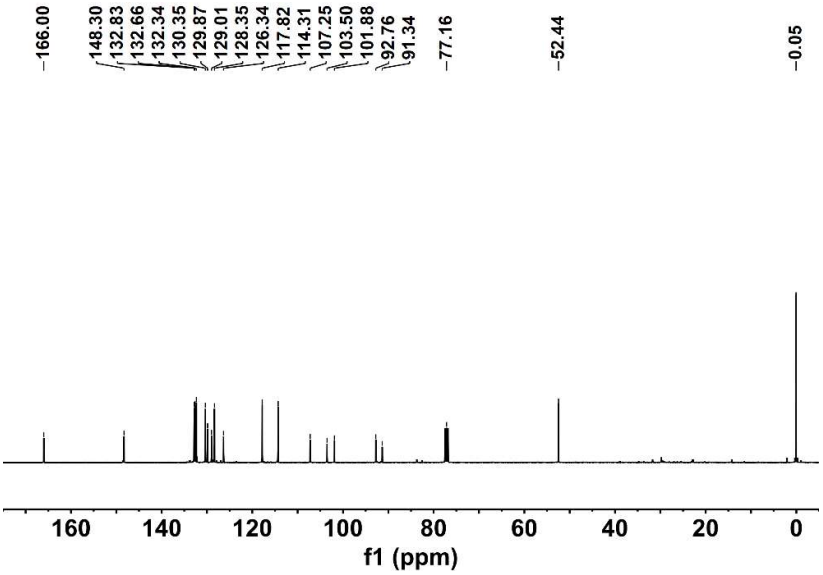

Fig. S4. The ^{13}C NMR spectrum of **SM4** ($CDCl_3$, 100 MHz).

Synthesis of methyl 3-((2-aminophenyl)ethynyl)-4-ethynylbenzoate (SM5).

A 50-mL round-bottom flask was charged with compound **SM4** (1.5 g, 4.3 mmol), anhydrous K_2CO_3 (1.79 g, 12.9 mmol) and a magnetic stirring bar. CH_2Cl_2 (10 mL) and methanol (10 mL) were added into the flask, and the reaction mixture was stirred at room temperature overnight.

Then the solvent was removed on a rotary evaporator and the residue was then dissolved in CH_2Cl_2. The organic mixture was extracted with CH_2Cl_2 (3 × 50 mL), washed with distilled water (3 × 100 mL) to remove the K_2CO_3, dried over anhydrous Na_2SO_4 and the solvent was removed by rotary evaporation to obtain compound **SM5** as red oily liquid (861 mg, 94.1% yield based on **SM4**). ^{1}H NMR (400 MHz, $CDCl_3$): δ = 8.13 (s, 1H), 7.85 (d, 1H), 7.53 (d, 1H), 7.33 (d, 1H), 7.09 (t, 1H), 6.66 (d, 1H), 6.64 (t, 1H), 3.86 (s, 3H), 3.43 (s, 1H). ^{13}C NMR (100 MHz, $CDCl_3$): δ = 165.99, 148.52, 132.82, 132.49, 132.33, 130.51, 130.40, 128.45, 127.95, 127.01, 117.95, 114.42, 107.20, 92.55, 91.63, 83.70, 82.58, 52.69.

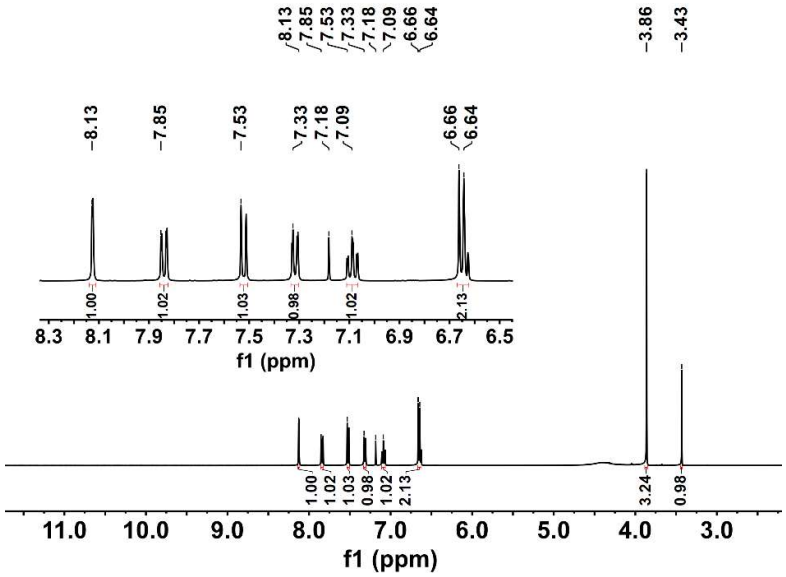

Fig. S5. The ^{1}H NMR spectrum of **SM5** ($CDCl_3$, 400 MHz).

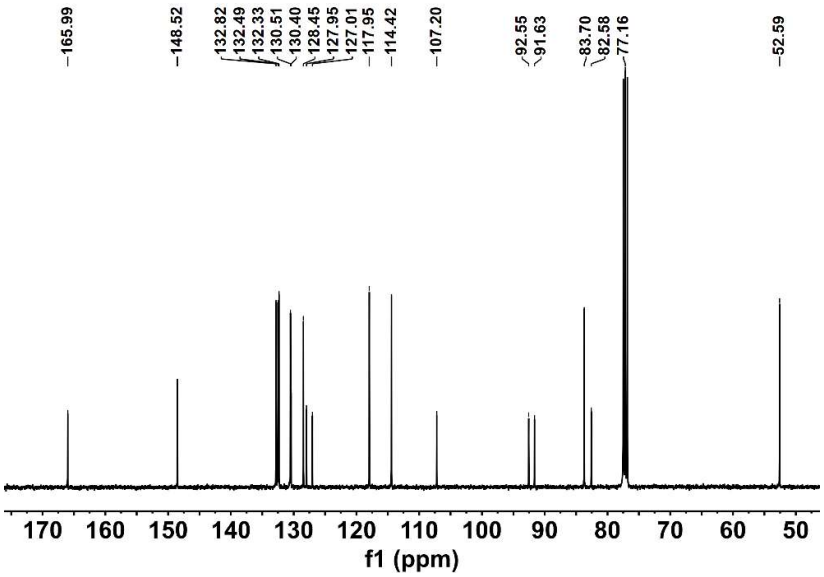

Fig. S6. The ^{13}C NMR spectrum of **SM5** ($CDCl_3$, 100 MHz).

Synthesis of dimethyl 4,4'-(buta-1,3-diyne-1,4-diyl)bis(3-((2-aminophenyl)ethynyl)benzoate) (Me_2L1).

A 50-mL round-bottom flask was charged with compound **SM5** (800 mg, 2.9 mmol) and anhydrous copper(II) acetate (1.58 g, 8.72 mmol). 20 mL acetonitrile were added into the flask and reacted at 70 ℃. At the end of the reaction, the green solid mixture was obtained by rotary steaming, washed with deionized water (3 × 200 mL) and extracted by CH_2Cl_2 (3 × 100 mL), dried over anhydrous Na_2SO_4 and the solvent was removed by rotary evaporation. The residue was purified by silica gel column chromatography (eluent: *n*-hexane/ethyl acetate, 4:1, v/v) to yield compound Me_2**L1** as the orange solid (701.4 mg, 44% yield based on **SM5**). ^{1}H NMR (400 MHz, $CDCl_3$): δ = 8.22 (s, 2H), 7.95 (d, 2H), 7.65 (d, 2H), 7.39 (d, 2H), 7.05 (t, 2H), 6.64 (t, 2H), 6.52 (d, 2H), 3.95 (s, 6H). ^{13}C NMR (100 MHz, $CDCl_3$): δ = 165.72, 148.55, 133.13, 132.57, 132.22, 130.76, 130.55, 128.31, 127.62, 126.94, 117.73, 114.41, 106.45, 92.53, 92.28, 82.91, 79.32, 52.58.

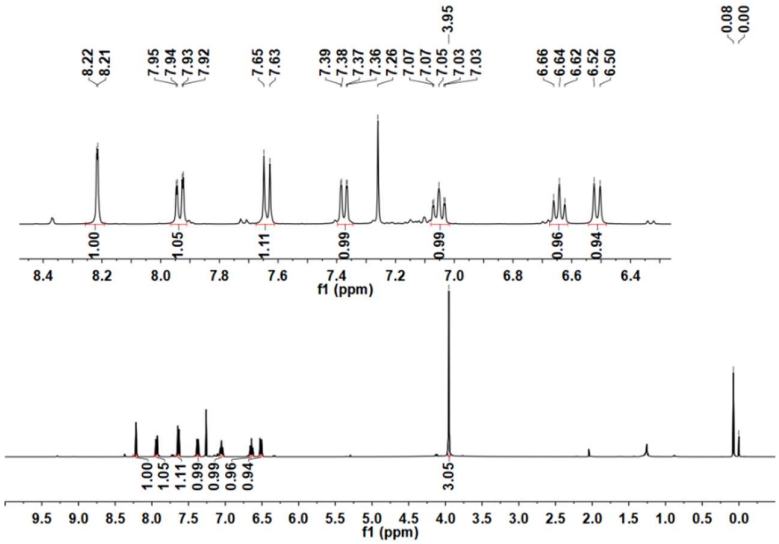

Fig. S7. The ^{1}H NMR spectrum of Me_2**L1** ($CDCl_3$, 400 MHz).

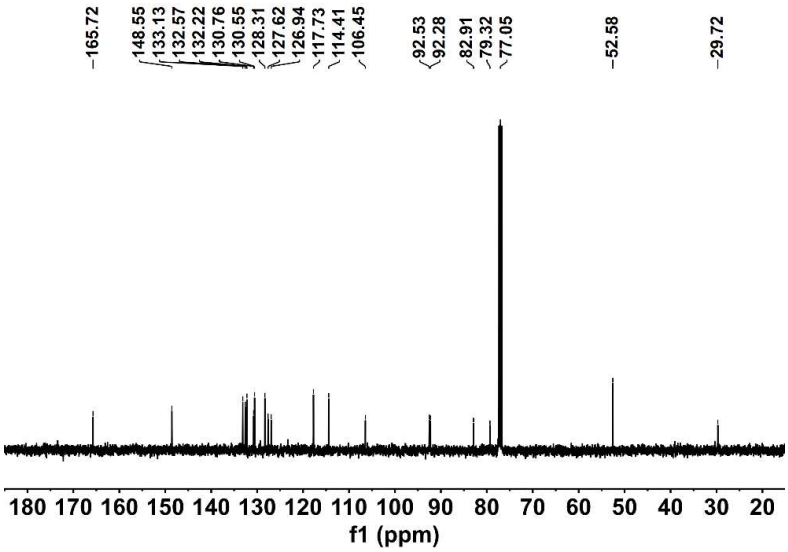

Fig. S8. The ^{13}C NMR spectrum of Me_2**L1** ($CDCl_3$, 100 MHz).

Synthesis of 4,4'-(buta-1,3-diyne-1,4-diyl)bis(3-((2-aminophenyl)ethynyl)benzoic acid) (H_2L1).

In a round bottom flask, Me_2**L1** (500 mg, 0.911 mmol) and KOH (18 mg, 18.22 mmol) were added. THF (10 mL) and deionized water (10 mL) were then added, and the reaction was stirred at 60°C for 24 hours. After cooling to room temperature, the resulting red solid mixture was obtained by removing the solvent using a rotary evaporator, and deionized water was added to the mixture, followed by the slow addition of HCl solution under stirring until the pH reached 2. The mixture was then filtered and washed with deionized water (3 × 200 mL), and finally vacuum dried. The product H_2**L1** was obtained as the orange solid (388.6 mg, 82% yield based on Me_2**L1**). ^{1}H NMR (400 MHz, DMSO-d_6): δ = 8.28 (s, 2H), 7.95 (d, 2H), 7.87 (d, 2H), 7.32 (d, 2H), 7.11 (t, 2H), 6.78 (d, 2H), 6.53 (t, 2H). ^{13}C NMR (100 MHz, DMSO-d_6): δ = 166.06, 148.43, 133.46, 132.28, 132.00, 130.70, 128.61, 127.11, 125.66, 117.15, 115.06, 105.65, 92.81, 91.67, 82.48, 78.69.

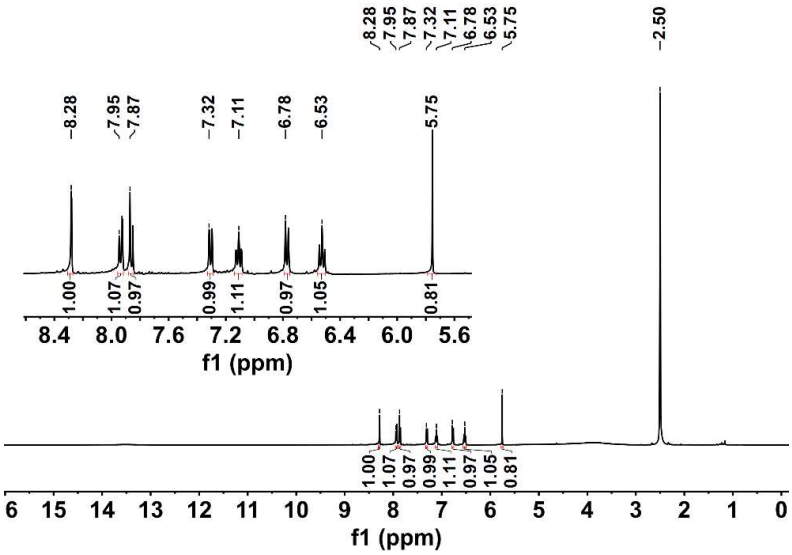

Fig. S9. The ^{1}H NMR spectrum of H_2**L1** (DMSO-d_6, 400 MHz).

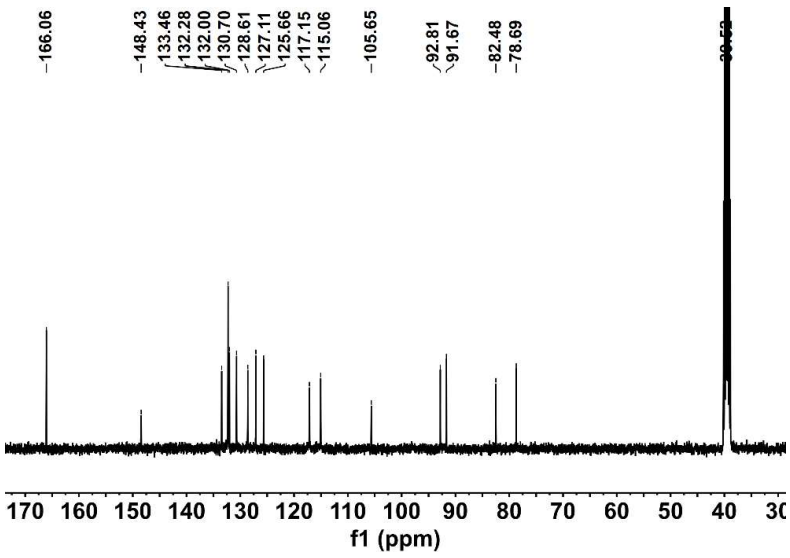

Fig. S10. The ^{13}C NMR spectrum of H_2**L1** (DMSO-d_6, 100 MHz).

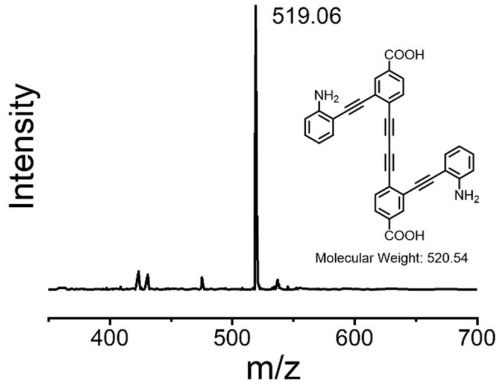

Fig. S11. A mass spectrum (ESI) of compound H_2**L1**.

Synthesis and activation of ZrL1.

H_2**L1** (3 mg, 5.77 mmol) and $ZrCl_4$ (1.6mg, 6.86 mmol) was loaded into a glass tube. Then HCOOH (24 μL) and *N*,*N*-dimethylformamide (DMF, 300 μL) mixed solution was added and the tube was sealed with an oxyhydrogen flame. The glass tube was placed in an oven at 90 °C for 48 hours, during which crystalline solid slowly formed. After the sealed tube was heated for 48 hours, it was cooled to room temperature over 4 hours. The yellow crystalline solid were collected and washed with DMF (15 mL) and acetone (15 mL) and air-dried to obtain yellow Zr**L1** crystalline solid. For elemental analysis, the Zr**L1** (50 mg) were activated *via* Soxhlet extraction with acetonitrile for three days, and then placed in vacuum at 80 °C for 10 hours. Elemental analysis found C (44.65%), H (3.17%) and N (2.78%) for Zr**L1**, this analysis fits the formula to be $Zr_6O_4(OH)_4(HCOO)_7(C_{34}H_{18}N_2O_4)_{2.5}(H_2O)_{11}$ (M_w 2488.97), which gives a calculated profile of C (44.40%), H (3.16%) and N (2.81%).

Structure simulation.

The structure model of Zr**L1** was constructed by the secondary building block of 6-connected $[Zr_4O_4(OH)_4]$ and 2-connected ditopic **L1**$^{2-}$ in reference to MOFs bearing **hxl** topology.[2-5] Using Materials Studio (v6.1.0) suit of programs by Accelrys, the model of Zr**L1** was generated with $P\bar{3}$ space group (No. 147) before replacing the linker (including the cell parameters and atomic positions) and subsequently Geometry Optimization by Forcite Calculation was carried out. To modify the lattice parameters to match the observed PXRD, Pawley refinement procedure was used, leading to trigonal lattice with $a = b = 23.938$ Å, $c = 9.537$ Å, $\alpha = \beta = 90^o$, $\gamma = 120^o$. Instrumental peak broadening parameters and additional profile parameters, background and crystallite size broadening were also used in the refinement to obtain the resultant structural model of Zr**L1**. The R_{wp} and R_p are equal to 4.54% and 2.80%, respectively (Fig. 2c).

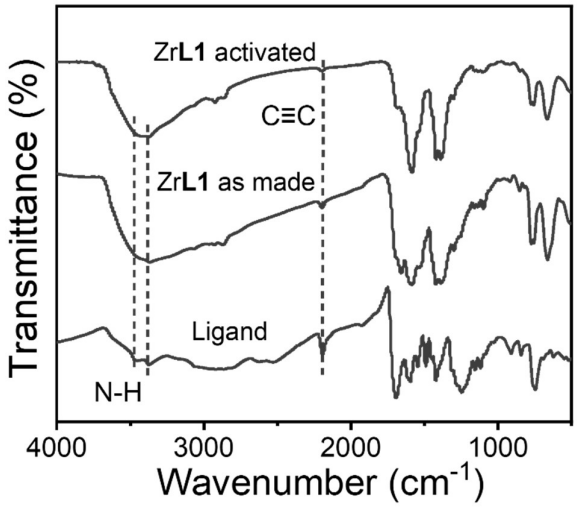

Fig. S12. FT-IR spectra of ligand, as made sample of Zr**L1** and activated sample of Zr**L1**.

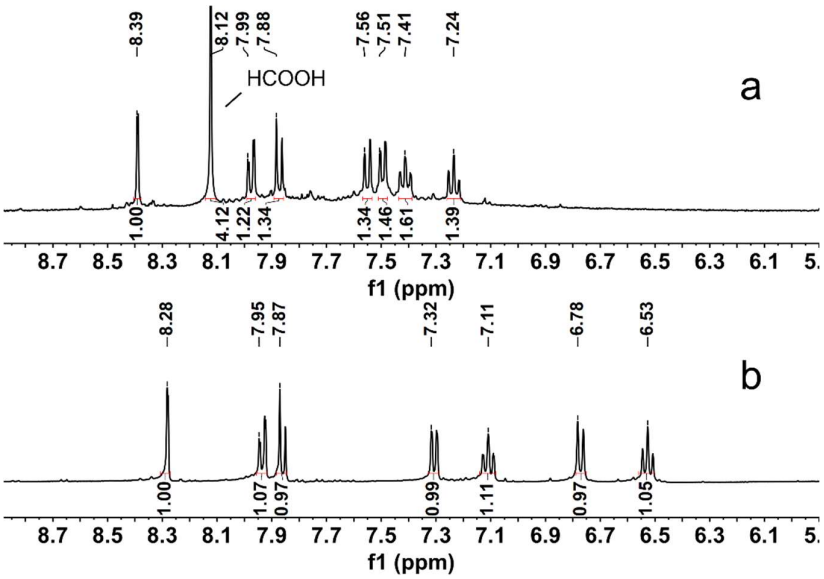

Fig. S13. ^{1}H NMR spectra of: (a) the filtrate of Zr**L1** digested in HF/DMSO-d_6; (b) H_2**L1** in DMSO-d_6.

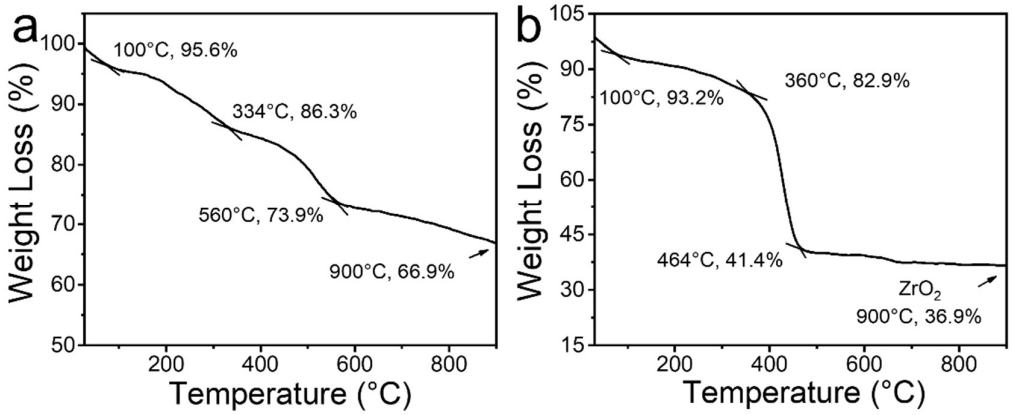

Fig. S14. Thermogravimetric analysis (TGA) plots of activated Zr**L1** (a) in N_2 and (b) in air.

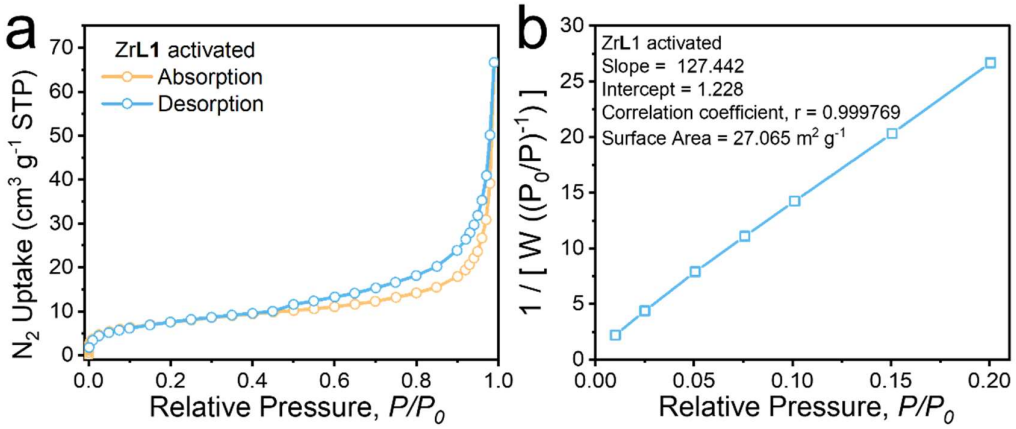

Fig. S15. (a) N_2 sorption isotherm at 77 K and (b) BET plot for activated Zr**L1** (outgassed at 100 ℃ under vacuum for 12 hours). N_2 sorption isotherm of Zr**L1** reveals a type-II gas sorption isotherm and QSDFT analysis gives BET surface area of 27.065 m^2 g^{-1}.

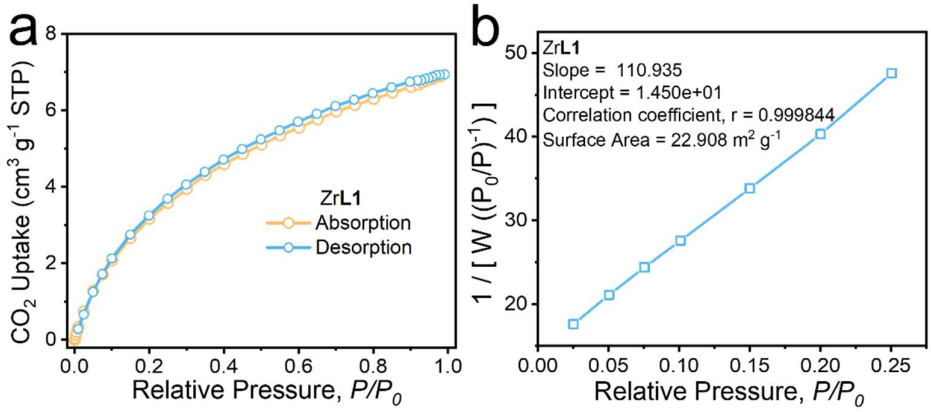

Fig. S16. (a) CO_2 sorption isotherm at 175 K and (b) BET plot for activated Zr**L1** (outgassed at 100 ℃ under vacuum for 12 hours). CO_2 sorption isotherm of Zr**L1** reveals a type-II gas sorption isotherm and QSDFT analysis gives BET surface area of 22.908 m^2 g^{-1}.

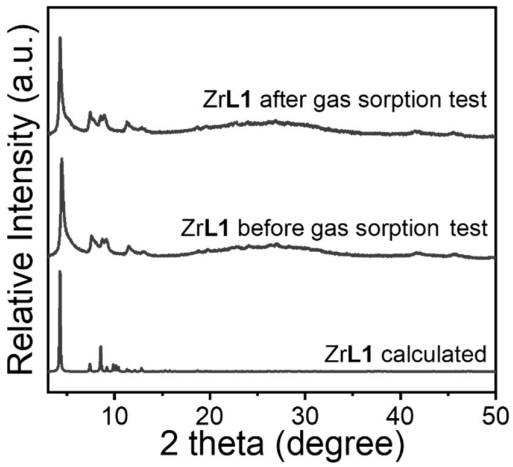

Fig. S17. PXRD patterns (Cu Kα, λ = 1.5418 Å) of Zr**L1** before and after gas sorption measurement.

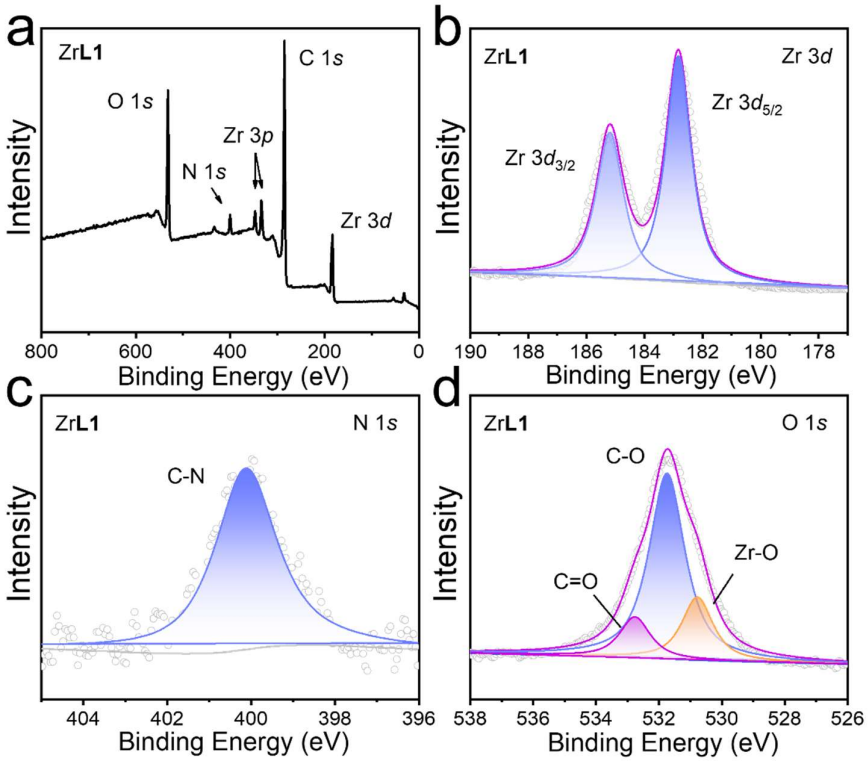

Fig. S18. XPS spectra of Zr**L1**: (a) Full region; (b) Zr 3*d* region; (c) N 1*s* region; (d) O 1*s* region. The powder samples were ground and pressed to form a thin pellet (~0.5×0.5 cm^2).

Element	Weight %	Atomic %
C K	56.97	77.03
N K	4.39	5.09
O K	13.14	13.34
ZrL	25.50	4.54

Fig. S19. EDS elemental analysis results of Zr**L1**.

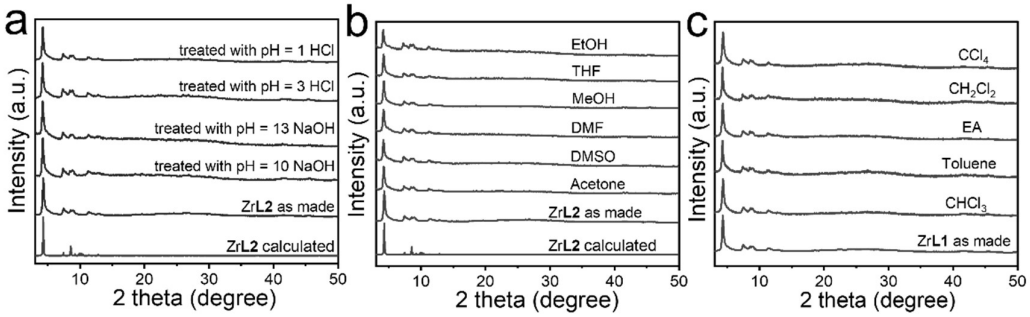

Fig. S20. PXRD patterns (Cu Kα, λ = 1.5418 Å) of as made Zr**L1** sample immersed in aqueous solutions of (a) pH = 1 and 3 (prepared by HCl solution), 10 and 13 (prepared by NaOH solution); (b, c) different solvents at room temperature for 24 hours.

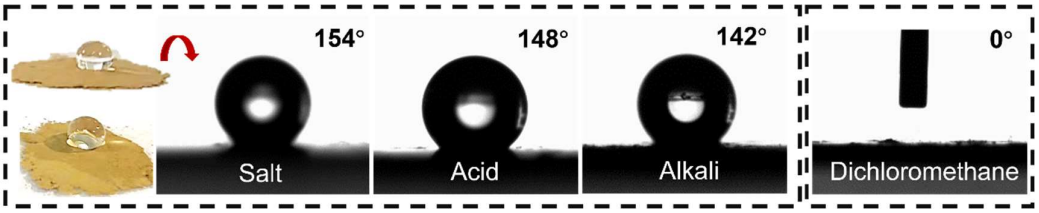

Fig. S21. Photographs of the droplets of saline water (3.5 wt.% NaCl, pH = 7), acidic solution (0.01 M HCl, pH = 2), alkaline solution (0.01 M NaOH, pH = 12) and dichloromethane on Zr**L1** powder with contact angle values.

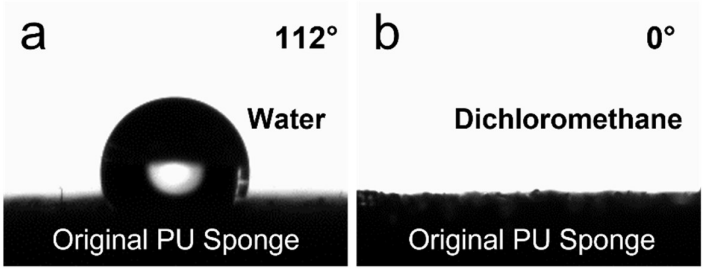

Fig. S22. Digital photographs of droplet profiles on the surface of original PU sponge with contact angle values.

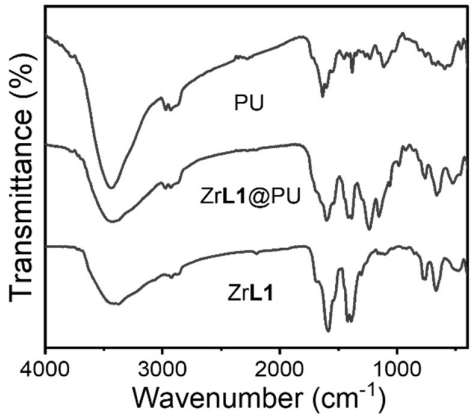

Fig. S23. FT-IR spectra of Zr**L1**, PU and Zr**L1**@PU.

Table S1. Loading of Zr**L1**@PU.

Zr**L1**	w_0 (g)	w_1 (g)	Loading content (wt.%)
10 mg	0.0798	0.1048	20.6
20 mg	0.0872	0.1157	31.1
30 mg	0.0863	0.1305	48.0

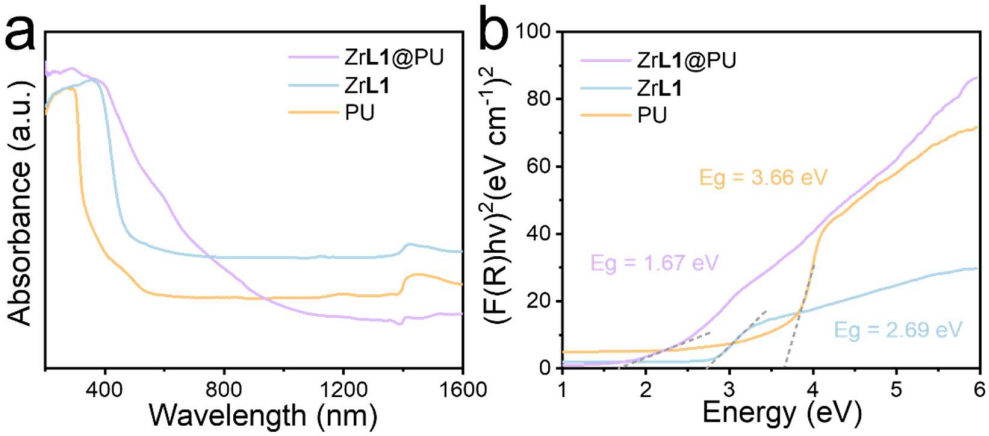

Fig. S24. (a, b) Kubelka-Munk-transformed reflectance spectra for solid samples of PU, Zr**L1**, Zr**L1**@PU.

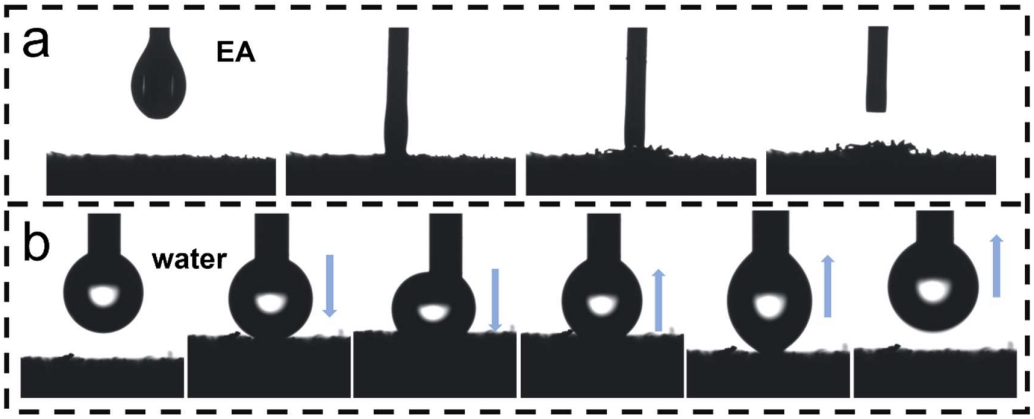

Fig. S25. The compression and detachment of (a) organic droplets and (b) water droplets on the surface of Zr**L1**@PU.

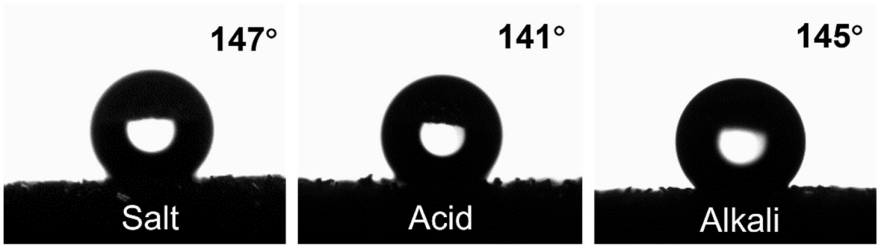

Fig. S26. Photographs of the droplets of saline water (3.5 wt.% NaCl, pH = 7), acidic solution (0.01 M HCl, pH = 2), alkaline solution (0.01 M NaOH, pH = 12) on Zr**L1**@PU with contact angle values.

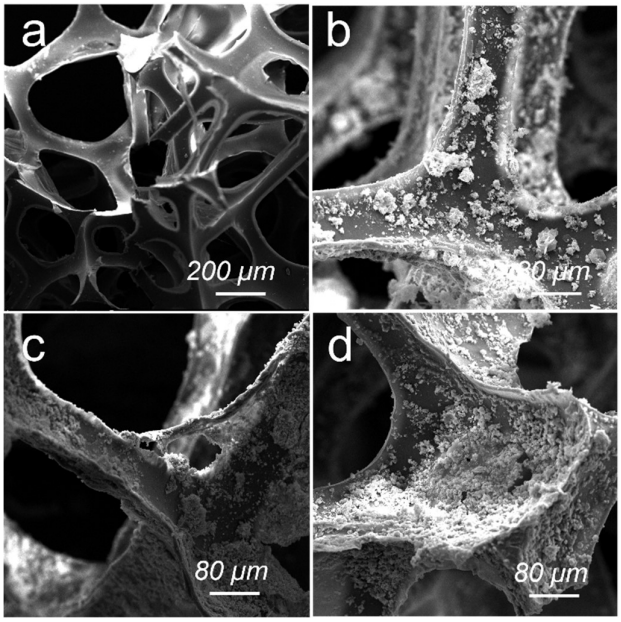

Fig. S27. SEM images of original PU Sponge (a) and Zr**L1**@PU samples with different loadings of Zr**L1** (10.0, 20.0 and 30.0 mg loadings for b, c and d).

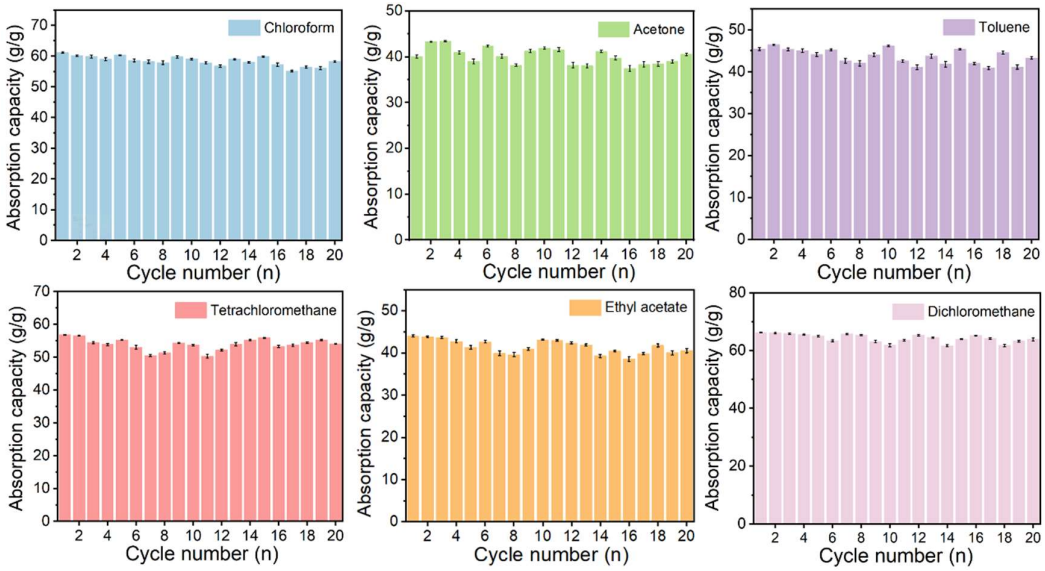

Fig. S28. Organic solvent-absorption capacities of the Zr**L1**@PU (the errors estimated to vary from ±1.4% to ±3.2%).

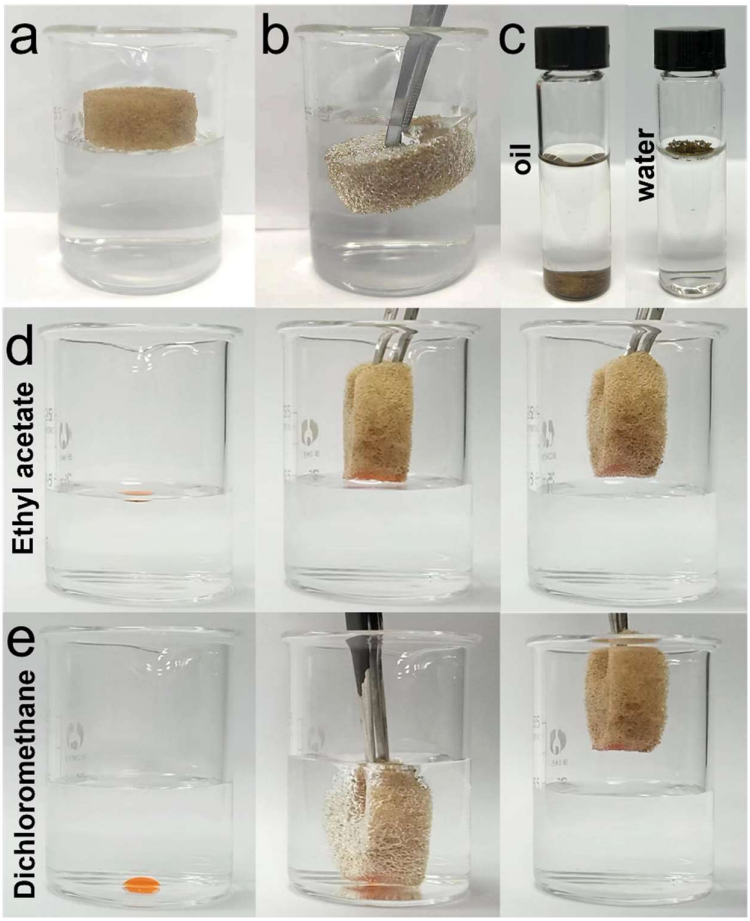

Fig. S29. (a, b) Photographs of Zr**L1**@PU in water; (c) Photograph of Zr**L1** powder in water and oil phase; Photographs showing the absorption of ethyl acetate (d) and dichloromethane (e) from water by Zr**L1**@PU.

Table S2. Absorption capacity, separation efficiency and flux of different kinds of oil.

Oil Types	Absorption capacity (g/g)	Separation efficiency (%)	Flux (L m^{-2} h^{-1})
Chloroform	61.09	99.3	5340
Acetone	43.43	96.2	3956
Tetrachloromethane	56.78	98.0	4611
Ethyl acetate	44.03	96.7	4420
Toluene	46.41	97.7	4570
Dichloromethane	66.19	98.8	4788

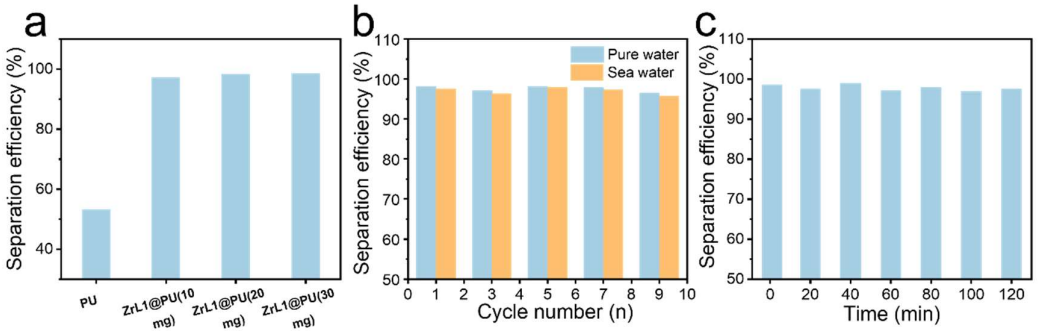

Fig. S30. The separation efficiency of (a) Zr**L1**@PU with different loadings in dichloromethane/water mixture; (b) dichloromethane/pure water or dichloromethane/sea water mixture for 9 cycles of separation; (c) Zr**L1**@PU in dichloromethane/water mixture as a function of operation time duration (the errors estimated to vary from ±1.6% to ±4.4%).

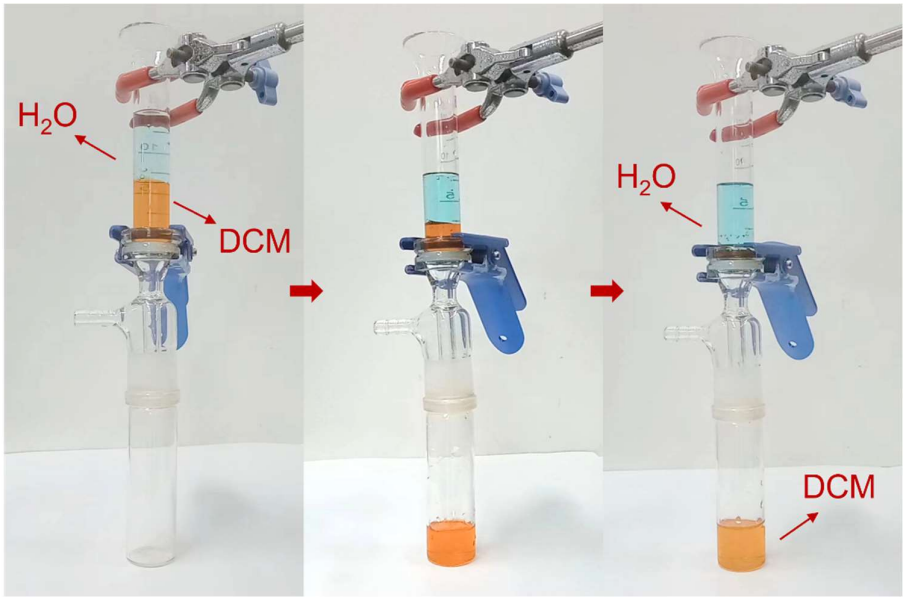

Fig. S31. The dichloromethane-water mixture separation process.

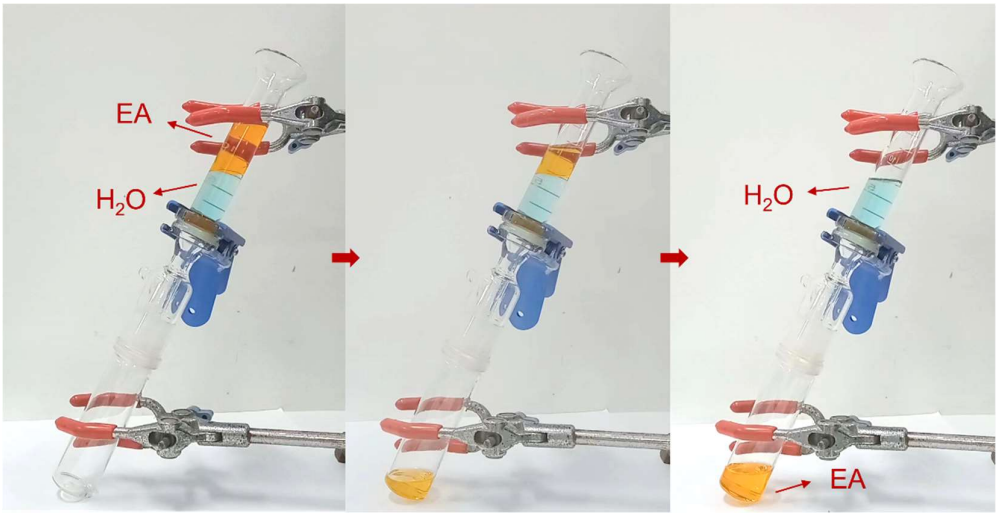

Fig. S32. The ethyl acetate-water mixture separation process.

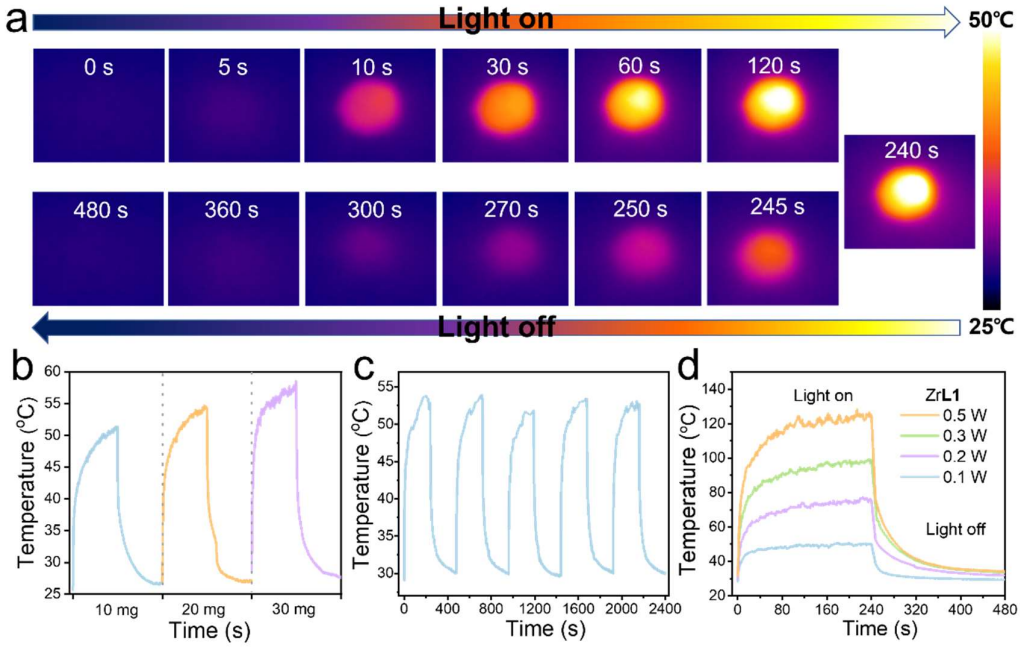

Fig. S33. (a) IR thermal images of Zr**L1** under xenon lamp (1.0 kW m^{-2}); (b) Photothermal conversion behaviour of Zr**L1** (different amounts) under one-sun irradiation within eight minutes; (c) Anti-photobleaching property of Zr**L1** during five cycles of heating–cooling; (d) Photothermal conversion behaviour of Zr**L1** under different light intensities (1.0, 2.0, 3.0 and 5.0 kW m^{-2}).

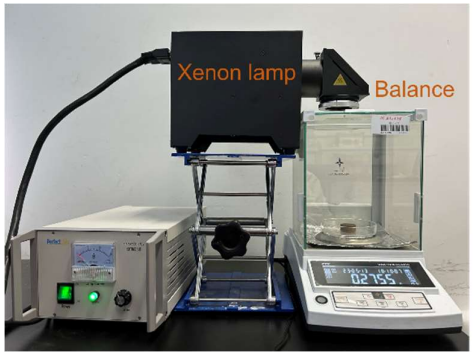

Fig. S34. Schematic diagram of photo-driven solvent evaporation experimental set-up.

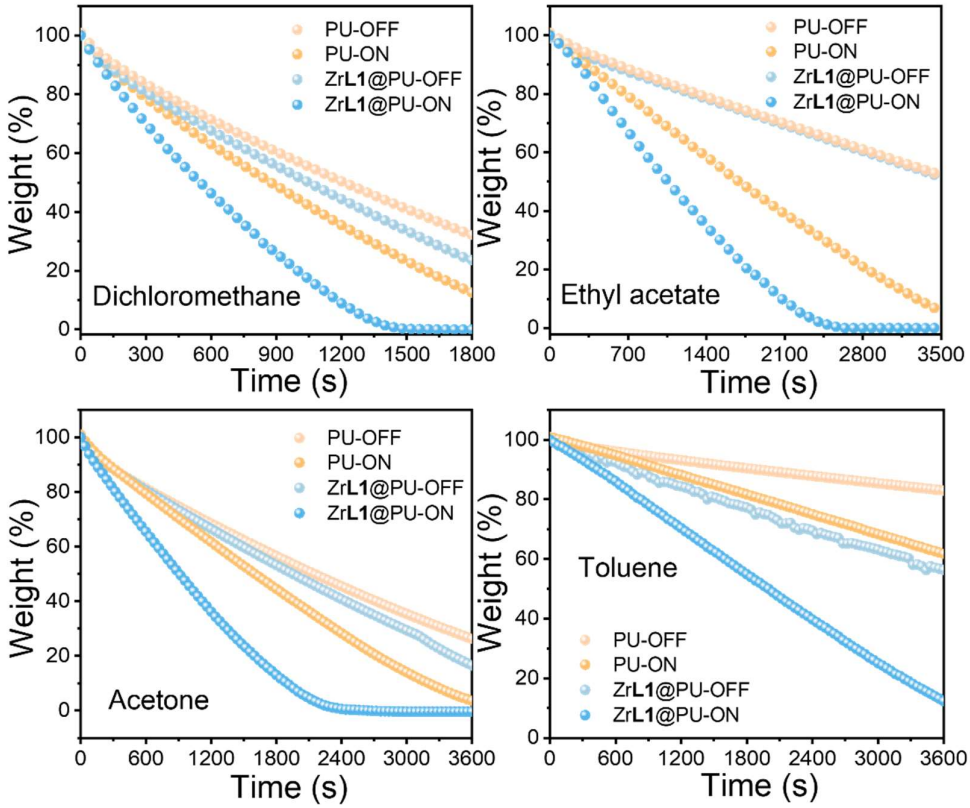

Fig. S35. Photo-driven distillation tests of Zr**L1**@PU. Weight variations of PU or Zr**L1**@PU saturated by dichloromethane, ethyl acetate, acetone and toluene with/without the light illumination at a power density of 1.0 kW m^{-2}.

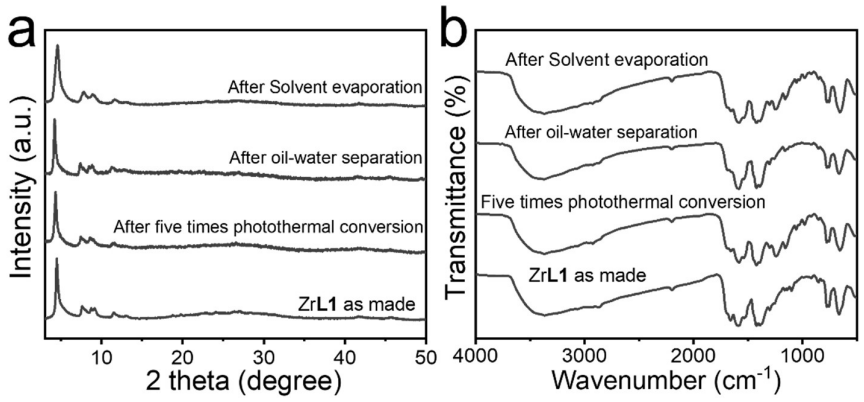

Fig. S36. (a) FT-IR spectra and (b) PXRD patterns of Zr**L1** recovered from Zr**L1**@PU by ultrasonication after five photothermal conversion cycles, oil/water separation and 20 cycles of solvent evaporation experiment.

Table S3. Comparisons of absorption capacities (in g/g) and separation efficiency (%) of some absorbents with Zr**L1**@PU

S. No .	**Absorbents**	**Absorption substances**	**Absorption capacity (g/g)**	**Separation efficiency (%)**	***Ref.***
1	Zr**L1**@PU	chloroform, acetone, diethyl ether, dichloromethane, toluene, tetrachloromethane, *n*-hexane	43.43–66.19	96.2–99.3	**This work**
2	SEnS	crude oil	22.59	90–99	*Ref.* 6
3	SHMOF-PP	diesel oil, petrol oil, kerosene, crude oil, dichloromethane, chloroform, carbon tetrachloride, ethyl acetate, hexane, toluene	28.28–38.93	95–99	*Ref.* 7
4	cotton fibre modified *via* the solgel method	diesel oil, lubrication oil, crude oil, peanut oil	25.61–57.01	98.5	*Ref.* 8
5	modified jute fibre *via* the sol-gel method	crude oil, diesel oil, lubricating oil, peanut oil	7.41–10.29	–	*Ref.* 9
6	PDMS/CB@PU	pump oil, edible oil, dichloromethane, toluene, ethyl acetate, hexamethylene, *n*-octane, ethyl alcohol, petroleum ether, isopropanol	28.5–68.7	>95	*Ref.* 10
7	polystyrene branched 9-octadecenoic acid grafted graphene	hexane, heptane, nonane, decane, hexadecane	11.00–27.00	–	*Ref.* 11

8	MOF-PU sponge	*n*-hexane, paraffin, ethanol, edible oil, DMF, carbon tetrachloride	29.00–56.00	>96	*Ref.* 12
9	UiO-66-F_4@rGO/MS	*n*-hexane, isooctane, dichloromethane, 1,3,5- trimethylbenzene, silicone oil diesel oil light diesel oil crude oil	26.00–61.00	99.73	*Ref.* 13
10	MOF@RGO composites	chloroform, *n*-hexane, silicone oil, bump oil, bean oil, toluene, acetone, butanone	14.00–37.00	50–80	*Ref.* 14
11	MOFs-copper foam	soybean oil, *n*-hexane, isooctane, gasoline, dichloromethane, chloroform	1.50–3.50	>96	*Ref.* 15
12	Macroporous silicone sponges	crude oil, sunflower oil, kerosene, diesel, alcohol, acetic acid, chloroform, acetone, diethyl ether, *n*-hexane, isooctane, dichloromethane	9.70–27.00	>99	*Ref.* 16
13	PVDF/SiO_2@GO nanofibrous aerogel	*n*-Hexane, kerosene, toluene, cooking oil, dichloromethane, chloroform	129–264	>99	*Ref.* 17
14	ZIF-8-PDA-Ag@MS	*n*-hexane, cyclohexane, dodecane, acetone, toluene, tetrahydrofuran, chloroform, chlorobenzene, diesel oil, pump oil, silicone oil, and corn oil.	85.45–168.95	>94	*Ref.* 18
15	SH-UiO-66@CFs	motor oil, silicone oil, gasoline, kerosene, toluene, hexane, ethyl acetate, carbon tetrachloride, chloroform, dichloromethane	27.14–49.27	95–98	*Ref.* 19

References.

1. Q. Xiao, M. Lu, Y. Deng, J.-X. Jian, Q.-X. Tong and J.-J. Zhong, *Org. Lett.*, 2021, **23**, 9303–9308.
2. J. Jia, A. J. Blake, N, R. Champness, P. Hubberstey, C. Wilson and M. Schröder, *Inorg. Chem.*, 2008, **47**, 8652–8664.
3. H. L. Nguyen, F. Gándara, H. Furukawa, T. L. H. Doan, K. E. Cordova and O. M. Yaghi, *J. Am. Chem. Soc.*, 2016, **138**, 4330–4333.
4. V. Sharma, D. De, S. Pal, P. Saha and P. K. Bharadwaj, *Inorg. Chem.*, 2017, **56**, 8847–8855.
5. W. Lin, E. Ning, L. Yang, Y. Rao, S. Peng and Q. Li, *Inorg. Chem.*, 2021, **60**, 11756–11763.
6. P. Cherukupally, W. Sun, A. P. Y. Wong, D. R. Williams, G. A. Ozin, A. M. Bilton and C. B. Park, *Nat. Sustain.*, 2020, **3**, 136–143.
7. C. Gogoi, A. Rana, S. Ghosh, R. Fopase, L. M. Pandey and S. Biswas, *ACS Appl. Nano Mater.*, 2022, **5**, 10003–10014.
8. N. Lv, X. Wang, S. Peng, L. Luo and R. Zhou, *RSC Adv.*, 2018, **8**, 30257–30264.
9. N. Lv, X. Wang, S. Peng, H. Zhang and L. Luo, *Int. J. Environ. Res. Public Health*, 2018, **15**, 969.
10. J. Chen, M. Sun, Y. Ni, T. Zhu, J. Haung, X. Li and Y. Lai, *J. Hazard. Mater.*, 2023, **445**, 130541.
11. F. I. Alghunaimi, D. J. Alsaeed, A. M. Harith and T. A. Saleh, *J. Clean. Prod.*, 2019, **233**, 946–953.
12. Z. He, H. Wu, Z. Shi, X. Duan, S. Ma, J. Chen, Z. Kong, A. Chen, Y. Sun and X. Liu, *Colloids Surf. A: Physicochem. Eng. Asp.*, 2022, **648**, 129142.
13. Y. Zhan, S. He, J. Hu, S. Zhao, G. Zeng, M. Zhou, G. Zhang and A. Sengupta, *J. Hazard. Mater.*, 2020, **388**, 121752.
14. J. Gu, H. Fan, C. Li, J. Caro and H. Meng, *Angew. Chem. Int. Ed.*, 2019, **58**, 5297–5301.
15. J. Du, C. Zhang, H. Pu, Y. Li, S. Jin, L. Tan, C. Zhou and L. Dong, *Colloids Surf. A: Physicochem. Eng. Asp.*, 2019, **573**, 222–229.
16. J. Cao, D. Wang, P. An, J. Zhang and S. Feng, *J. Mater. Chem. A*, 2018, **6**,18025–18030.
17. X. Wang, Z. Liu, X. Liu, Y. Su, J. Wang, T. Fan, X. Ning, S. Ramakrishn and Y.-Z. Long, *Carbon*, 2022, **193**, 77–87.
18. Y. Zhang, S. Hou, H. Song, G. Qin, P. Li, K. Zhang, T. Li, L. Han, W. Liu and S. Ji, *J. Hazard. Mater.*, 2023, **451**, 131064.
19. R. Dalapati, S. Nandi, C. Gogoi, A. Shome and S. Biswas, *ACS Appl. Mater. Interfaces*, 2021, **13**, 8563–8573.